ICARUS 108, 225–233 (1994)

The Distribution of Water Frost on Charon

MARC W. BUIE

Lowell Observatory, 1400 W. Mars Hill Rd., Flagstaff, Arizona 86001
E-mail: buie@lowell.edu

AND

SCOTT K. SHRIVER

Stanford University, Stanford, California 94305

Received August 30, 1993; revised December 6, 1993

We present high-spatial-resolution imaging observations of the Pluto–Charon system taken with ProtoCAM on the IRTF. Our dataset consists of measurements from eight nights at widely separated rotational longitudes and covering five wavelengths—standard J, H, and K, plus two special narrow band filters at 1.5 and 1.75 μm. The relative flux contributions of Pluto and Charon were extracted, when possible, by fitting a two-source Gaussian image model to the observed images. At K, we find the Charon–Pluto magnitude difference to be on average 1.8 mag, somewhat less than the value of 2.2 mag found by Bosh *et al.* (1992, *Icarus* 95, 319–324). The average differential magnitude at 1.5 and 1.75 μm is 2.0 and 1.6, respectively. The larger magnitude difference at 1.5 μm is due to a water-frost absorption band on the surface of Charon. Our observations are consistent with a surface of Charon dominated by water frost at all longitudes.

INTRODUCTION

Our knowledge of Pluto and its satellite, Charon, has increased dramatically in the past 10 years despite their small size and remote location in the outer solar system. One reason for these advances, despite observational difficulties, is the six-year season of mutual eclipses and occultations between Pluto and Charon that concluded in 1991. These events have played a key role in unlocking information that would otherwise require a spacecraft flyby, such as system mass and relative sizes (e.g., Tholen *et al.* 1987).

The synchronous rotation of Pluto and Charon limits mutual-event-derived results, such as separate spectral properties, to a single hemisphere of each object. The first such result was the tentative identification of water frost from four-band infrared photometric observations by Marcialis *et al.* (1987). Shortly thereafter, Buie *et al.* (1987) obtained a more detailed spectrum of the sub-Pluto hemisphere of Charon confirming a surface dominated by water frost. It is quite reasonable to assume that water frost is globally distributed on the surface of Charon. Marcialis and Lebofksy (1991) presented the first evidence to support the conclusion of a global distribution on the basis of the variations seen in the combined spectra with rotation. Recent advances in infrared technology combined with a growing awareness of the quality of the observing site at Mauna Kea provide an opportunity to make spatially resolved observations at longitudes other than those covered by mutual event observations.

Previous work by Bosh *et al.* 1992 (hereafter referred to as BEL) presented spatially resolved photometry of Pluto and Charon in the K band (2.2 μm). While this filter often leads to the best images of the system, the results are somewhat hard to interpret since the filter bandpass is much broader than the absorption features from methane and water frost known to exist on Pluto and Charon. The work we present here provides similar measurements in standard bandpasses (J, H, and K) as well as adding two special filters at 1.5 and 1.75 μm that are specifically diagnostic of methane and water frost absorptions.

OBSERVATIONS

The observations for this project were performed during two runs at NASA's 3-m Infrared Telescope Facility (IRTF) atop Mauna Kea, Hawaii, using an infrared array camera known as ProtoCAM (Toomey *et al.* 1990). The ProtoCAM instrument is a hybrid indium antimonide (InSb) CCD device, formatted into a 62 × 58 pixel array. ProtoCAM was designed specifically with performance in the thermal IR (3–5 μm) in mind, but it is sensitive over the entire 1–5 μm range.

Presented at the conference "Pluto and Charon," Flagstaff, AZ, July 1993.

0019-1035/94 $6.00

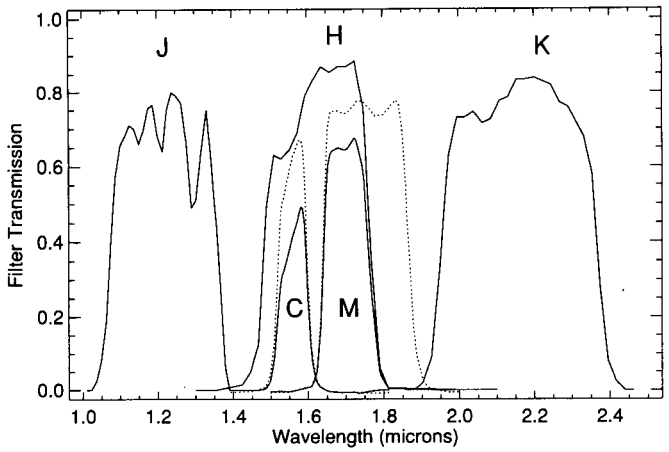

FIG. 1. Filter transmission curves. Standard J, H, and K filters are shown, as well as curves for the two special filters meant to discriminate between the 1.75-μm methane band (M) and nearby continuum (C). The dotted curves show the actual tracings for the special filters at room temperature. The solid curves for the special filters are the product of the H filter profile and the C or M filter curves giving the filter profile for the combination.

Observations were made with three standard filters, J, H, and K, and two of special design. Our first special filter was sensitive to the 1.7-μm absorption band of methane: its bandpass was roughly 1.6–1.8 μm. The other special filter corresponded to a continuum level between two methane absorption bands, though it was also sensitive to the 1.5-μm absorption band of water frost. The bandpass of the continuum filter was 1.5–1.6 μm. The special filters we used could not be mounted in the Dewar, thus requiring a nonstandard cardboard mount just outside the dewar window. To eliminate the thermal emission from the filters themselves, we always used the internal (cold) H filter as a thermal blocking filter. The bandpasses of the special filters were optimized with respect to the Pluto spectrum, assuming they would be used at the detector temperature (77°K or below). Outside the Dewar the temperature of the filter is considerably warmer (near 273° K) and leads to a band center shifted by ~0.2 μm to the blue. Figure 1 shows the transmission curves for the filters we used. The curves shown for the special filters are tracings made at room temperature and thus most closely correspond to the conditions under which the filters were used.

ProtoCAM features a variable platescale from 0.135 to 0.35 arcsec/pixel (8- to 20-arcsec field of view). We made all our observations at the minimum possible plate scale (0.135) to ensure adequate sampling of the Pluto–Charon image even under the best seeing conditions. However, this decision compromised our ability to derive absolute photometry due to the small field of view.

All exposures are taken as an object–sky frame pair of equal duration. We chose an exposure time of 3 min as a compromise between getting as many source photons as possible in a single frame and minimizing the effects of image drift from poor tracking or large excursions in seeing. The sky frame was always taken 20 arcsec south of the object position.

TABLE I
Summary of Observations

UT Date	Time	J	H	K	CH_4	Cont	Phot	Seeing
1991 May 06	10:49–15:49	–	–	4	–	–	no	1.3″
1991 May 09	09:34–15:45	1	1	18	–	–	yes	0.8″
1992 May 08	05:31–15:40	5	5	14	3	3	yes	1.1″
1992 May 09	05:18–15:10	5	5	8	4	4	yes	0.9″
1992 May 10	05:20–15:56	4	3	12	6	4	yes	1.0″
1992 May 11	05:17–15:43	1	1	12	2	2	no	1.1″
1992 May 12	06:05–15:09	–	–	17	–	–	no	0.9″
1992 May 13	09:48–15:00	2	1	4	8	6	yes	1.1″

Table I enumerates the observational periods, their general photometric results, and the breakdown of frames per filter. Table II contains information regarding the geometric circumstances at the time of observation: distance to the Earth and Sun from Pluto, solar phase angle, sub-Earth latitude and longitude on Pluto, apparent separation and position angle of Pluto and Charon, and the pixel offsets from Pluto to Charon in our images. The latitude and longitude coordinate system used for Pluto and Charon is the system defined by Buie *et al.* 1992. Figure 2 shows the times of observation in the context of the known lightcurve of the Pluto–Charon system and the apparent separation between Pluto and Charon as a function of sub-Earth longitude.

The 1991 observing run was only partially allocated to our high-resolution imaging program to demonstrate the feasibility of resolving the Pluto–Charon system. At that time, few people felt the resolution was high enough at these shorter wavelengths to make the project feasible. For this reason, we concentrated on K-band imaging to establish the potential of the technique. The 1991 May 6 data were plagued by high winds, clouds, and poorer seeing and only minimal information at K was obtained.

TABLE II
Observational Circumstances

UT Date	r (AU)	Δ (AU)	α (°)	Sub-Earth Lat.	Sub-Earth Long.	Sep (″)	P.A. (°)	dx (pixels)	dy (pixels)
1991 May 06	29.673	28.702	0.54	7.5	260	0.93	172	−1.0	6.8
1991 May 09	29.673	28.700	0.53	7.4	96	0.94	350	1.2	−6.8
1992 May 08	29.697	28.724	0.53	9.6	42	0.64	1	0.0	−4.8
1992 May 09	29.698	28.723	0.52	9.6	343	0.31	141	−1.4	1.8
1992 May 10	29.698	28.722	0.52	9.5	287	0.90	167	−1.5	6.5
1992 May 11	29.698	28.722	0.51	9.5	235	0.78	177	−0.3	5.8
1992 May 12	29.698	28.722	0.51	9.5	177	0.16	280	1.2	−0.2
1992 May 13	29.698	28.722	0.52	9.5	116	0.85	346	1.6	−6.1

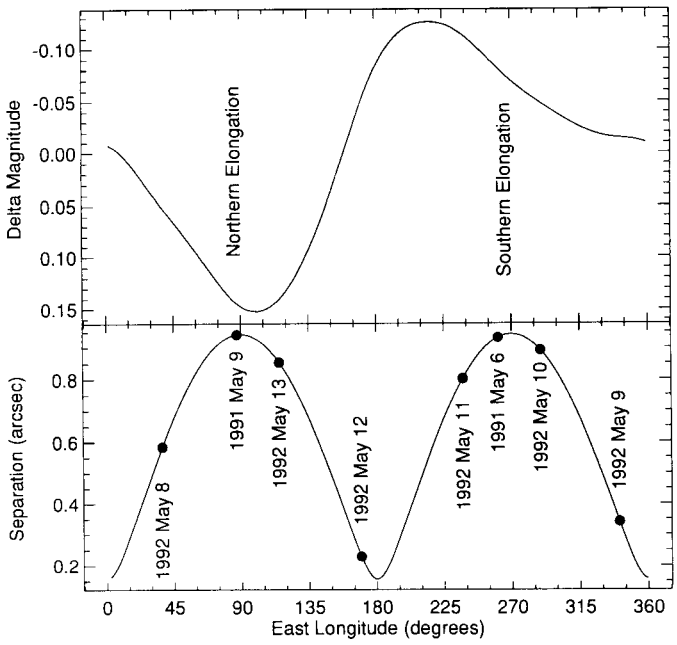

FIG. 2. Context of observations. The bottom panel contains a plot of the apparent separation of Pluto and Charon as a function of the sub-Earth longitude. Superimposed on the curve are the times of the observations presented in this paper. For reference, the visible lightcurve is shown in the top panel. The observations provide a reasonable, if sparse, coverage of the entire lightcurve.

The night of 1991 May 09 afforded excellent seeing conditions as well as optimal separation of Pluto and Charon.

On the strength of the 1991 May 09 observations we were allotted additional time in 1992 to continue the project. The 1992 observations varied in quality over the 6-day observing run. May 11 and 12 were marked by clouds and high winds. Fortunately, May 12 corresponded to a minimal separation between Pluto and Charon. Of these nights, only one had seeing as favorable as during the previous year. Unfortunately, the best night of seeing coincided with a Pluto–Charon separation of 0.16 arcsec and yielded no information. May 10 provided the best combination of good seeing and separation in the 1992 dataset.

Recurrent instrumental problems also impeded the acquisition of useful images. The focus of the telescope usually was seen to drift during the night and required numerous focus sequences to maintain optimum focus. A more formidable problem was that of adjusting the gate voltage for the array. Residual images at the 3–10% level were not uncommon with the recommended gate voltages as well as with other improper settings. We found it necessary to increase the gate voltage to diminish the residual image problem, which sharply increased the dark current in quite a few pixels, often rendering those pixels useless. This situation lead to more than the usual number of bad pixels scattered randomly in the array. Even more vexing was the capricious stability of any gate setting. The gate voltage had to be checked each night for an optimal compromise between residual image and excessive dark current. The telescope itself contributed to some of our difficulties. An apparent failure of the mirror support system caused the image quality to deteriorate very rapidly once the object passed 30 min west of the meridian. Other images were lost due to poor tracking. In the end, these difficulties did not affect the data other than to limit the amount we could collect within the allotted time. We mention these problems as a warning that such high resolution imaging observations are often limited by several factors other than seeing, particularly on Mauna Kea, where the seeing is typically quite good.

REDUCTIONS

We converted all raw ProtoCAM images to calibrated images with the following ordered steps: subtraction of an average bias frame, linearization correction, division by a flat field image. Next, each object/sky frame pair is then differenced eliminating most, if not all, of the sky signal. In the final step we remove all bad pixel values from the images.

The average bias frame is constructed from the simple average of images read in rapid succession from the detector while a cold dark slide covers the detector. This step determines the electronic bias of the detector read-out system, which is present in all images.

The linearization correction attempts to remove the effects of the slightly nonlinear response of the detector to indident light. Unlike optical CCDs, ProtoCAM suffers a slight nonlinear response to incident light that becomes more pronounced at high signal levels. The correction is determined from a sequence of images taken with varying signal level. A second-order polynomial was fit to each pixel to determine its own linearization correction. For consistency, this correction was applied to all frames even though the correction was negligible for all the Pluto–Charon frames.

The flat field response images were constructed from images taken of the dome. In contrast to optical CCDs, there is a large scattered light component accompanying the flat fielding illumination that comes from thermal emission from all parts of the dome and telescope. To remove this, we took sets of images first with the dome lights on and then with the dome lights off. The difference between these image pairs is the desired flat field response image.

The final image correction was the replacement of bad pixel values. For each object/sky frame pair, the sky frame was examined to find deviant pixels. The brightest and darkest 10% of the sky pixels were removed and then the standard deviation was computed. The omitted pixels

included the deviant pixels sought and removing them ensured a reliable measurement of the true noise in the sky frame. Next, any pixels found to be more than 4σ from the median of the entire sky frame were marked as bad. Each pixel in the list was then replaced by the average of its neighbors *after* the sky frame from the object frame. This process removed nearly all the bad pixels from the image and left a cosmetically perfect image that could then be processed by normal photometry software without regard to outliers. The bad pixels identified were stable during a night. While observing, we kept Pluto and Charon away from these bad pixels, ensuring that the repaired pixels were either in the wings of the PSF or farther away. The effect of the bad pixel removal was largely cosmetic and made the extraction of the photometry much easier but in the end had little effect on the answers derived.

Due to the small size of the ProtoCAM array, a maximum aperture of 2 arcsec could be achieved with conventional aperture photometry. To achieve better photometric results, the data were modeled to fit Gaussian forms. Relative fluxes could then be derived through simple analytic integration. This method follows closely that of BEL who attempted to fit the point-spread functions (PSF) to both Lorentzian and Gaussian forms. Their results suggested negligible differences between the two forms, and thus we opted for the more simple Gaussian form.

For stellar images our model had five free parameters: background counts (1), location and peak value of the object (3), and the width of the Gaussian PSF (1). For the Pluto–Charon system the model gains one free parameter, the peak value of the Charon PSF. The model needs only one additional parameter because the position of Charon on the chip can be computed from its ephemeris and an accurate determination of the array platescale and orientation. Due to the extremely small separation of Pluto and Charon, the PSFs of the two objects should be characterized by the same width. Figures 3 and 4 provide an example of our data set and the ability of our two-source model to match the observations. Figure 3 is an overview of the entire data set at K sorted in order of increasing longitude. In this set of images, the nights of 1991 May 09 and 1992 May 10 clearly stand out as having the best resolved images of the system. The images in Fig. 4 are all from 1992 May 10 and show data from all filters we used. Reproductions on paper are less convincing than image display devices but during reduction of the data the continuum filters were quickly recognized where Charon all but disappears compared to the other filters. The residual patterns seen in these images are due to very slight tracking errors during the exposures.

The orientation and platescale were determined from observing an asteroid (482 Petrina) move across the field of view while guiding on an off-axis field star. The known ephemeris of Petrina was used to find the best fit scale and orientation. The results of this fit verified that the nominal scale and orientation were good to 1% and thus the nominal values were adopted.

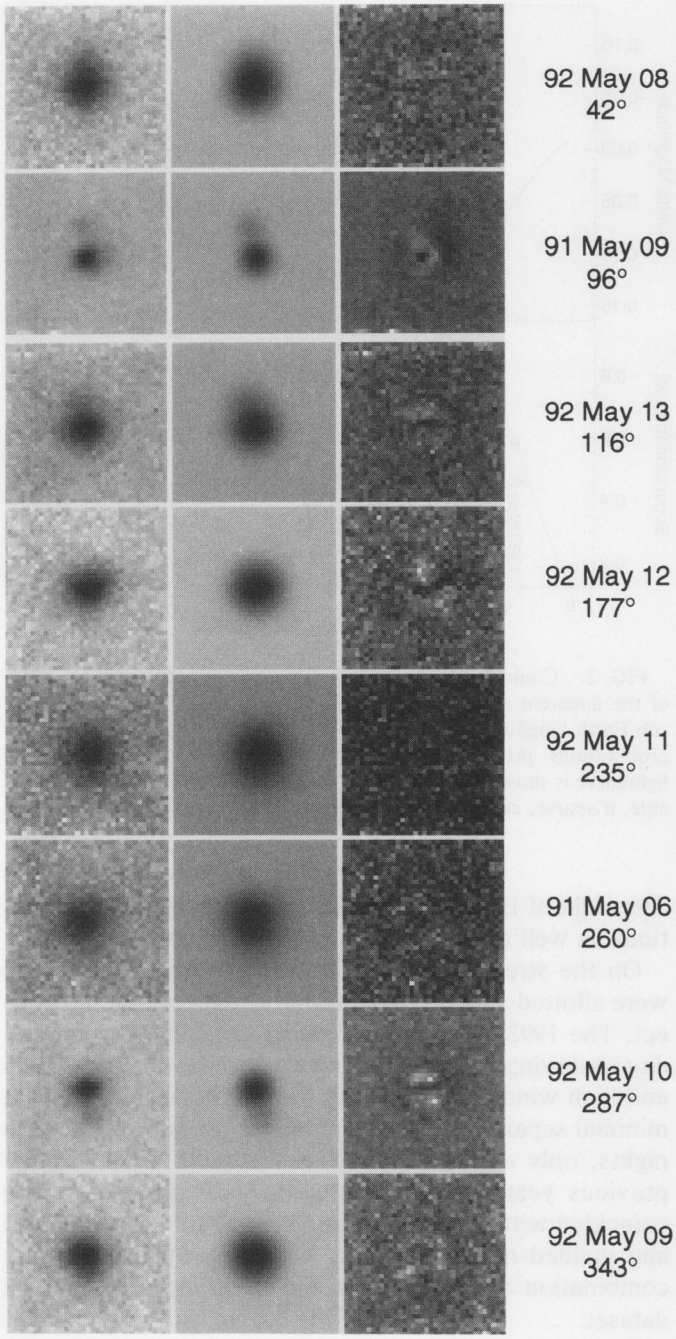

FIG. 3. Sample K data. These images depict the best K-band data from each night. The images are ordered by increasing longitude from top to bottom. Image orientation is as seen in the plane of sky, with north to the top and east to the left. The left column is the observed image, the middle column is the two-source model image, and the right column is the residual image (data − model) multiplied by a factor of 4 relative to the data and model.

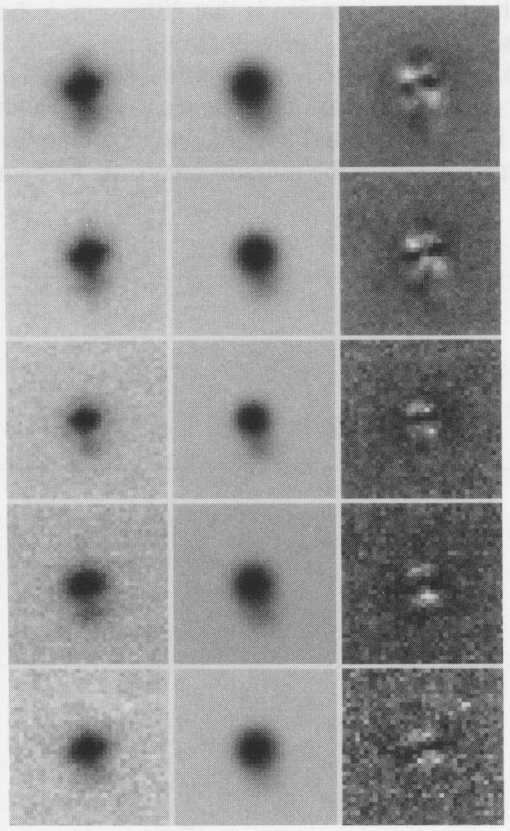

FIG. 4. Sample data versus wavelength. This set of images shows representative data from 1992 May 10 for each wavelength observed. The three columns are shown in a manner similar to the previous figure. Note the slight variations in seeing between filters where the trend is to have poorer seeing at shorter wavelengths. Also note how much fainter Charon appears in the continuum filter.

TABLE III
Charon–Pluto Differential Magnitudes

UT Date	Filter	Δm	σ	N_{obs}
1991 May 06.406	K	2.21	0.12	3
1991 May 09.528	J	1.65	0.05	1
.528	H	1.64	0.07	1
.728	K	1.62	0.10	15
1992 May 08.348	J	1.95	0.60	5
.421	H	2.15	0.16	5
.407	K	2.35	0.68	5
.361	CH_4	2.43	0.38	2
1992 May 10.380	J	1.78	0.16	4
.505	H	1.75	0.19	3
.173	K	1.76	0.41	12
.503	Cont.	2.18	0.42	4
.476	CH_4	1.63	0.33	6
1992 May 11.328	J	2.27	0.29	1
.324	H	2.88	0.85	1
.487	K	1.64	0.15	6
.333	CH_4	1.96	0.96	1
1992 May 13.411	J	1.37	0.38	2
.452	H	1.49	0.12	1
.450	K	1.60	0.34	4
.390	Cont.	1.91	0.39	4
.536	CH_4	1.64	0.25	8

The ephemeris we adopted for Charon is the same used by Buie *et al.* 1992. More current orbital parameters exist, as provided by Null *et al.* 1993 and Young *et al.* 1994. The low-precision data presented here are insensitive to these recent refinements and we felt the older orbit was adequate for our purposes.

The reduction of the absolute photometry produced little definitive information about the combined Pluto + Charon lightcurve due to our exceedingly large error bars. The error bars associated with the differential photometry were significantly smaller. Due to the smaller relative error and the interesting nature of the results, the remainder of this paper shall focus on the differential photometry.

RESULTS

The final results from this reduction are tabulated in Table III. The UT dates listed are the midtime of the average of all measurements on each night. The tabulated values are averages of all measurements where the Charon–Pluto differential magnitude was determined to better than 1.5σ. This condition is equivalent to using only those observations that represent clear detections of Charon in the data. No useful Δm measurements could be extracted from the data on 1992 May 9 or 12 when the separation was 0.31 and 0.16 arcsec, respectively.

Figures 5 and 6 show the final results in graphical form in two different ways. Figure 5 shows each night of data separately as a function of wavelength for those nights where more than one filter was used. For reference, the solid curve is the Charon–Pluto spectrum from Buie *et al.* 1987 at a longitude of 180°. Figure 6 shows the data from each wavelength separately as a function of the sub-Earth longitude. For comparison, the visible lightcurve at the epoch of observations as derived from the model of Buie *et al.* (1992) is shown at the top of Fig. 6 but at a greatly expanded vertical scale compared to the Δm data. In both figures, the filled circles indicate final points made from the average of three or more independent measurements and should have more reliable error bars. The hollow circles come from fewer than three measurements and the uncertainties are correspondingly less precise. Also shown in Fig. 6 are the data from BEL, as hollow triangles.

The best indicator of the quality of the night is the ratio of the Pluto–Charon separation to the FWHM of the image. The data from the nights of 1991 May 9 and 1992 May 10 are substantially better than the rest. The poorest night that yielded data was 1992 May 8. On that

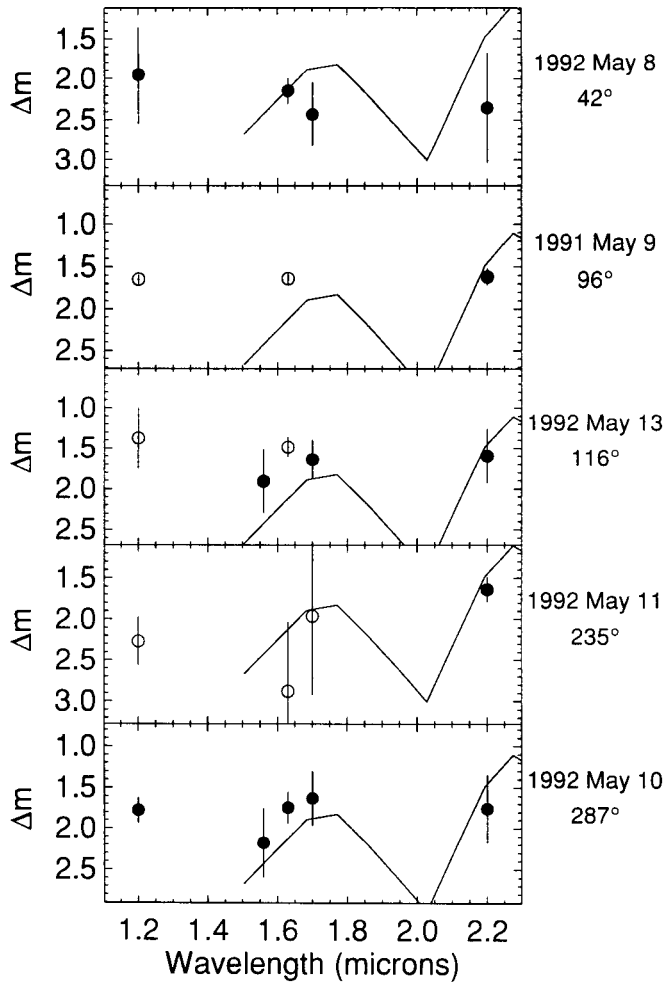

FIG. 5. Charon–Pluto differential photometry versus wavelength. These six panels show the differential photometry for all nights where a sensible measurement was made in more than one filter. The plots are ordered in increasing sub-Earth longitude with the date and longitude labeled on the right. Data plotted with filled circles are averages of three or more points.

night the seeing was not particularly good and the separation was smaller. The correspondingly larger uncertainties are the result of the poorer conditions.

The best temporally sampled wavelength is the K band. There are also four measurements from BEL with which to compare our results. The agreement between the two datasets is not particularly good. In particular, one of our best nights of data (1992 May 10, 287°) falls at almost exactly the same longitude as two of the BEL points and yet the measured Δm values differ by 0.8 magnitudes at all of J, H, and K wavelengths. Also, the behavior of Δm versus longitude does not show the same pattern of variation reported by BEL.

There are two simple explanations for the differences in the results. One explanation is that either one or both of the datasets are invalid. There is no objective evidence from which to support or refute this possibility. Taken at face value, one is left to assume some measure of validity in the two works. A second possible explanation is that the true uncertainties in the measurements are being un-

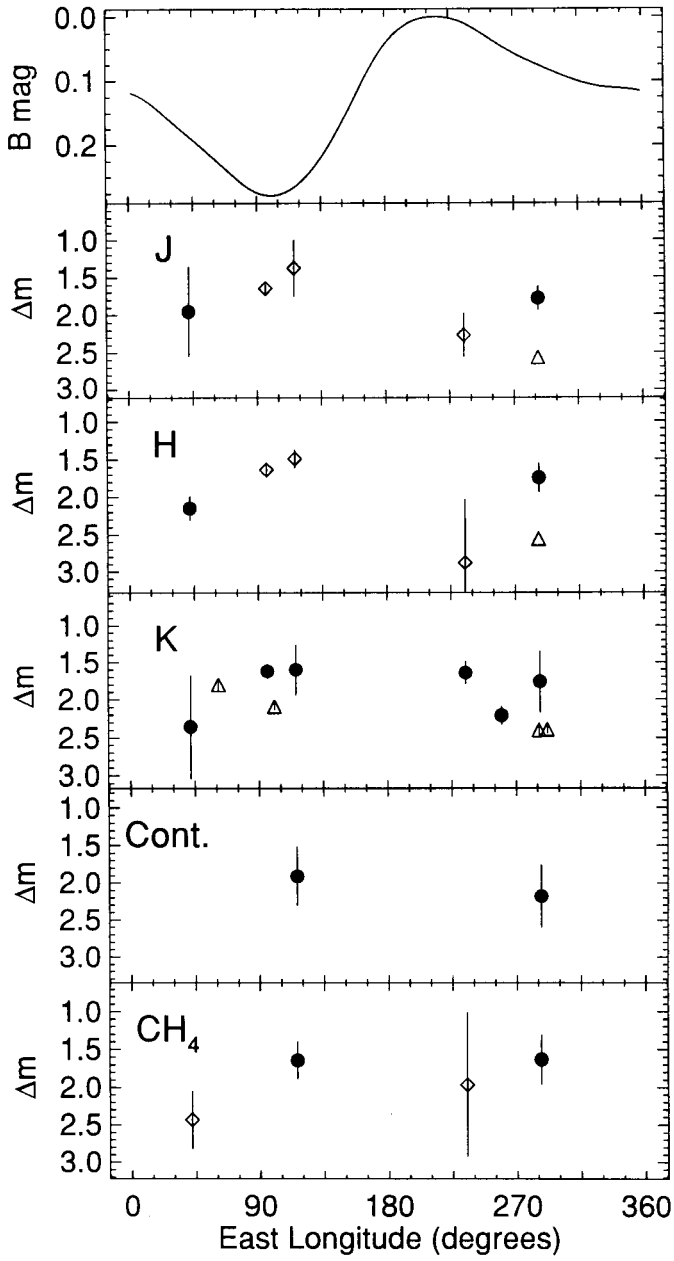

FIG. 6. Charon–Pluto differential photometry versus longitude. The top panel is a reference visual lightcurve for the combined Pluto–Charon system. The bottom five panels show the Charon–Pluto magnitude for each filter as a function of longitude. Filled circle points are averages of more than three points, hollow diamonds are two or fewer, and the triangles represent the Bosh *et al.* 1992 measurements.

derestimated. Given the nature of this difficult photometric extraction, it is not hard to imagine the uncertainties could be wrong. An alternative to these two explanations is a substantial temporal and rotational variability in the brightnesses of Pluto and Charon for which there is no other evidence. Temporal variations can probably be excluded on the basis of prior detailed photometric observations in the visible. Longitudinal variations are still possible but the data shown in Fig. 6 do not offer any clear pattern with rotation. Our new data indicate that the longitudinal scatter in Δm is approximately 0.5 mag, in contrast to the 1.0 mag value suggested by BEL.

Apparently, there are processes which are not reflected in the random errors derived from the data itself that can confuse the measurement of the relative brightnesses of Pluto and Charon. In an attempt to explain these discrepancies, we devised a series of tests to check the quality of extraction for the two PSF fits. We created synthetic two-point-source Gaussian images with noise. These synthetic images were processed with the same extraction software to find the best-fit values for the positions and the relative brightnesses of the sources. The BEL measurements left Charon's position floating where we chose to fix the position. We found no evidence for any systematic differences between letting the fainter source position be a free parameter and leaving it fixed to the known value. The only difference noted is a slightly larger set of cases where no solution is found when Charon's location is a free parameter. These cases are readily recognized by having unrealistic fitted values. It seems unlikely that the BEL results are affected in this way.

The remainder of our tests concentrated on fits leaving the Charon position as a known quantity. Figure 7 shows an excerpt from our synthetic image photometry tests. As expected, the fitting should and does get noisier as the separation gets small compared to the seeing. However, there is no evidence for any systematic error in the photometry. The only trend is that the random noise gets higher with poorer resolution. Note that with the one exception, all of our data are at a poorer resolution than the BEL data. An examination of the fitting error versus object separation (in pixels) also shows no strong systematic photometric error though the noise does get worse as the separation decreases. In this case, our data are much better separated than the BEL data due to the different plate scale used.

Another test was to look for systematic error in the fitted results versus the known relative brightness. Over the range of Δm of interest, there are again no systematic trends, just a general increase in scatter as the relative brightness increases. Perhaps the most telling result is the error versus FWHM in pixels. The BEL results are right at the edge of critical sampling (FWHM = 2 pixels) and the noise from the fitting is much larger as the image scale

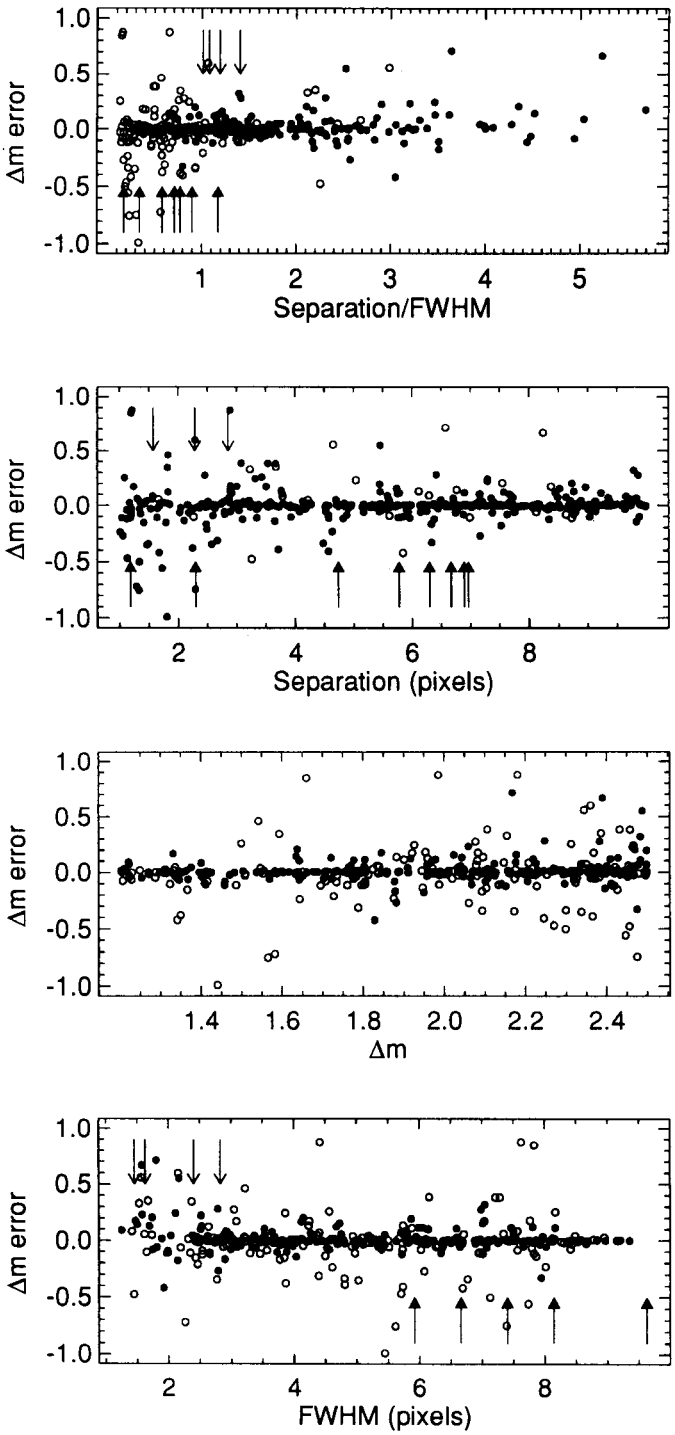

FIG. 7. Model-fitting errors for synthetic Pluto–Charon data fits. The ordinate is the difference between the known Pluto–Charon magnitude difference and the fitted difference for the two Gaussian PSF fit. In the top and bottom two panels, the hollow circles are for values of the Pluto–Charon separation less than 5 pixels, filled circles are greater than 5 pixels. In the second panel, the hollow circles are for values of FWHM less than 2.0 (undersampled images). The down-pointing arrows indicate where the Bosh *et al.* 1992 measurements fall within the sampled parameter space. The upward-pointing arrows indicate where our new observations fall.

approaches undersampling. However, this increase in the error appears to once again be a random effect. There is no systematic trend with image scale. Since the BEL results do come from the average of a number of measurements, there is still no explanation for the discrepancy between our measurements. Considering the results from our new observations, the conclusion of BEL that there is a large (~1 mag) variation in Δm_K versus longitude no longer seems plausible.

Returning to the spectral results plotted in Fig. 5, the best results are from the nights of 1991 May 9 and 1992 May 10, which should not be too surprising, since these two nights had the best conditions. The data from 1992 May 11 are too sparse to be of much use in our analysis. The data from 1992 May 8 and 1992 May 13, while slightly noiser, are still consistent with the mutual event spectrum of Charon–Pluto. The data from 1992 May 8 do seem to indicate that Charon is much darker than Pluto at all wavelengths for this longitude relative to all others measured, but the uncertainties are larger as well.

Concentrating on the 1992 May 10 data, are the data consistent with what we know about Pluto and Charon? To answer this question we constructed a simple model of the spectra of Pluto and Charon. For the spectrum of Charon, we chose the spectrum of Ariel from Brown and Cruikshank (1985). Miranda is actually a better match to the known spectrum of Charon but the known spectrum of Miranda does not extend down to 1 μm. To get a better match of the Ariel spectrum to Charon, we scaled the reflectance spectrum of Ariel by subtracting 0.7 and multiplying by 0.85 to increase the amount of water frost absorption. The combined spectrum of Pluto and Charon has been very well measured by Marcialis and Lebofsky (1991). We chose to use the average of *all* of their spectra to get a representative combined spectrum. With these analogs it is easy to reproduce the observed Δm from 1992 May 10. The level of the 1991 May 9 data is also easily matched by a 15% increase in the brightness of Pluto (holding Charon constant). This change is consistent with the known change seen in the visible lightcurve.

The measurements on 1992 May 10 and May 13 are very similar to the mutual event color ratio between the methane and continuum filters at very different sub-Earth longitudes. The observed continuum-to-methane ratio is thus consistent with the global distribution of water frost on Charon. The ratio would invert if water frost were to be removed altogether. Even a neutral ratio would indicated some water since we know methane to be global on Pluto.

CONCLUSIONS

Our observations are consistent with a water-frost covered surface of Charon at 116° and 287° longitude. Combined with the mutual event assisted detections (Buie *et al.* 1987, Marcialis *et al.* 1987) at 180° and the results of Marcialis and Lebofsky (1991), these results strengthen the case for global water frost on Charon. However, our data are not of sufficient quality to determine the details of any variations with longitude. The primary limitations are insufficient spatial resolution and insufficient field of view. Extraction of differential fluxes from the Pluto–Charon system seems to work much better in the visible, where the field of view is much larger (L. Young, private communication). Perhaps these measurements could be improved upon with a similarly large field of view in the infrared so on-chip field stars can be used to determine an empirical PSF.

Our K-band data seem to refute the notion of a large differential lightcurve between Pluto and Charon as proposed by BEL. However, this band is not particularly well suited for studying either surface, and the presence or lack of a lightcurve at K is not very diagnostic. The K band seems to be a popular wavelength to measure the Pluto–Charon system because it is the longest wavelength standard bandpass in which the system can be detected. Given the trend of improved seeing with increasing wavelength normally seen at the IRTF, the choice of K is obvious. In the future, investigations should utilize narrower bandpasses (or spectra) that isolate and measure the contributions from water frost and methane. Our efforts in this work are a step in the right direction with special methane and continuum filters. Finally, future progress in studying the distribution of volatiles on the surfaces of Pluto and Charon will not come without substantial improvements in detector and telescope technology such as that expected with the new imaging system and tip–tilt correction currently under development at the IRTF.

ACKNOWLEDGMENTS

This work was supported by NASA Planetary Astronomy Grant NAGW-2880. The authors were visiting astronomers at the Infrared Telescope Facility, which is operated by the University of Hawaii under contract with NASA. SKS was supported by The John Motley Morehead Foundation.

REFERENCES

Bosh, A. S., L. A. Young, J. L. Elliot, H. B. Hammel, and R. L. Baron 1992. Photometric variability of Charon at 2.2 μm. *Icarus* **95,** 319–324.

Brown, R. H., and D. P. Cruikshank 1985. The moons of Uranus, Neptune and Pluto. *Sci. Amer.* **253,** 38–47.

Buie, M. W., D. P. Cruikshank, L. A. Lebofsky, and E. F. Tedesco 1987. Water frost on Charon. *Nature* **329,** 522–523.

Buie, M. W., D. J. Tholen, and K. Horne 1992. Albedo maps of Pluto and Charon: Initial mutual event results. *Icarus* **97,** 211–227.

MARCIALIS, R. L., G. H. RIEKE, AND L. A. LEBOFSKY 1987. The surface composition of Charon: Tentative identification of water ice. *Science*, **237,** 1349–1351.

MARCIALIS, R. L., AND L. A. LEBOFSKY 1991. CVF spectrophotometry of Pluto: Correlation of composition with albedo. *Icarus* **89,** 255–263.

NULL, G. W., W. M. OWEN, JR., AND S. P. SYNNOTT 1993. Masses and densities of Pluto and Charon. *Astron. J.* **105,** 2319–2335.

THOLEN, D. J., M. W. BUIE, R. P. BINZEL, AND M. L. FRUEH 1987. Improved orbital and physical parameters for the Pluto–Charon system. *Science* **237,** 512–514.

TOOMEY, D. W., M. A. SHURE, E. M. IRWIN, AND M. E. RESSLER 1990. ProtoCAM—An innovative IR camera for astronomy. In *Proceedings of SPIE Conference 1235—Instruments in Astronomy VII,* p. 69.

YOUNG, L. A., C. B. OLKIN, J. L. ELLIOT, D. J. THOLEN, AND M. W. BUIE 1994. The Charon–Pluto mass ratio from MKO astrometry. *Icarus* **108,** 186–199.